Planet. Space Sci., Vol. 39, No. 4, pp. 617–626, 1991
Printed in Great Britain.

0032-0633/91 $3.00+0.00
Pergamon Press plc

THE MEASUREMENT OF ATOMIC OXYGEN IN THE MESOSPHERE AND LOWER THERMOSPHERE

WILLIAM E. SHARP
Space Physics Research Laboratory University of Michigan, Ann Arbor, MI 48109, U.S.A.

(*Received in final form* 1 *October* 1990)

Abstract—A discussion of the laboratory calibration, calibration simulation, and accuracy of a resonance fluorescence instrument for measuring oxygen atoms is given. The discussion demonstrates that a sensor can be calibrated with good accuracy to obtain *in situ* measurements of the oxygen density in the mesosphere/lower thermosphere. Oxygen data are reported from six rocket flights. These data represent four midlatitude flights and two auroral flights. There are two night and two day profiles for the midlatitude experiments. The maximum densities found from these sets of data in the 90–100 km regions are between 1.5×10^{11} cm^{-3} and 3.5×10^{11} cm^{-3}. Agreement with the MSIS-86 model predictions is obtained for altitudes above 120 km for midlatitude flights. The auroral data are less than the model prediction by about a factor of 2. The data show structure that is probably indicative of gravity wave effects of a nominal 5 km vertical wavelength.

INTRODUCTION

Accurate measurements of atomic oxygen densities in the mesosphere and lower thermosphere are a long standing problem. The atomic oxygen density is an important parameter in quantifying the dynamics and chemistry in this region of the atmosphere (Garcia and Solomon, 1985). The mesopause–lower thermosphere is the transition region from a mixed gas to a diffusively separated gas. The resulting change in particle mean free path is from centimeters to meters. The particles do not recognize that a physical object is in their midst when the mean free path is several times the size of the object. This renders *in situ* measurements by rocket difficult in this region because the nose of rockets is generally tens of centimeters or less. Those measurements by rocket-borne instruments that have been made appear to give diverging values for the oxygen density. A review by Offerman *et al.* (1981) of atomic oxygen measurements prior to 1980 indicated that the published values for the absolute atomic oxygen density at its maximum ranged over a factor of 40. This variation might be attributed to differences in experimental technique but even within the same technique, results vary widely. For example, using the resonance fluorescence technique, some recent experimenters have reported peak O densities near or below 10^{11} cm^{-3} (e.g. Howlett *et al.*, 1980; Dickinson *et al.*, 1987) while others have reported values in the range $5–20 \times 10^{11}$ cm^{-3} (e.g. Greer *et al.*, 1986; Dickinson *et al.*, 1980; Thomas and Young, 1981). Despite much debate (Llewellyn *et al.*, 1986; Llewellyn, 1988; Sharp, 1985, 1986), there exists no consensus as to what extent these differences are geophysical or instrumental in nature.

In situ measurements of [O] in the transition region suffer from the effects of the shock wave on the sampling process by the supersonic motion of the rocket. The flow of air over the probe is near-continuum near the mesopause and free molecular in the thermosphere above about 140 km. Examples of these flow effects have been described by Bird (1988). A discussion of an experimental approach to overcome the difficulties has been given by Sharp (1980). The resonance fluorescence module and its calibration were described. Its deployment on a 100 cm boom near the front of the payload is used to overcome the shock effects of the blunt-nosed payload. The angle of attack on both upleg and downleg is near zero so that wake effects are avoided. Some initial density results were also reported.

Given the rather large range of density values reported it is apparent that in the measurement of the atom density the absolute calibration of the sensor is critical. This report gives a full discussion of the calibration process for a resonance fluorescence instrument used by the author and the results are compared with a simulation of the instrument. The errors involved in this are also discussed at length. Additionally, the [O] profiles obtained in a number of experiments are also presented to show the variability in the magnitude and shape of the [O] profile. Comparisons with MSIS-86 (Hedin, 1987) are also discussed. Siskind and Sharp (1991, this issue) also discuss these measured profiles in the context of their deduction from airglow data.

CALIBRATION

A resonance fluorescence experiment requires knowledge of the absolute photon flux from the

source, the scattering volume, effective absorption cross-section, and instrument efficiency. Individually, these are difficult numbers to deduce with any accuracy. If, however, the scattering volume can be immersed in a flow of a known concentration of the atoms in question, then the ratio of detector count rate to the atom concentration (the calibration factor) for a given relative source flux is obtained. So long as near single scattering in the medium is applicable, source self-absorption is not significant, and source photon flux levels for flight and calibration are the same, then the experiment can make absolute concentration measurements. The present instrument was calibrated on a flow reactor in the laboratory before and after each flight. It is this laboratory-determined calibration that is applied to the data, not the theoretical estimates that are discussed below. The laboratory calibration removes the uncertainties in knowing the particulars of the source line shape and the volume excitation rate in the source.

Sharp and Kita (1987) derived an expression for the detector count rate as a function of the calibration factor for this instrument when the source of emission is a single line. For the case of a multiplet the count rate is given by

$$S_o = C(E)[O] \tag{1}$$

with the calibration factor given by

$$C(E) = \{\Sigma_i \int_\lambda E_i(\lambda)\sigma_i(\lambda)\,d\lambda\}\{A\varepsilon T\eta\}L, \tag{2}$$

where $E_i(\lambda)$ is the photon flux of the ith line at the scattering volume in photons $cm^{-2}\ s^{-1}$, $\sigma_i(\lambda)$ is the atomic absorption cross-section in square centimeters, A is the detector aperture, ε is the detector collection efficiency, T is the optical transmission of the detector optics, η is the quantum efficiency of the cathode, and L is the scattering length over which photons are emitted along the detector field of view. The summation enters because the oxygen emission consists of the 1302, 1305, and 1306 Å transitions from the common ^3S upper state to the three lower states $^3P_2$, $^3P_1$, and $^3P_0$, respectively.

It is well known that optically thin plasma discharge lamps exhibit Doppler emission profiles (e.g. Kaufman and Parkes, 1970). Assuming the absorption cross-section is the same for each line, the convolution integral can be written as

$$\int E_i(\lambda)\sigma_i(\lambda)\,d\lambda = \sigma_0\{D_a^2/(D_a^2+D_e^2)\}^{0.5}\langle E_i\rangle \tag{3}$$

$$= \sigma_0\{T_a/(T_a+T_e)\}^{0.5}\langle E_i\rangle, \tag{4}$$

where σ_0 is the absorption cross-section at line center which can be calculated if the oscillator strength of the transition is known. $\langle E_i\rangle = \int_\lambda E_i(\lambda)\,d\lambda$ is the lamp flux at the line i. D_a and D_e are the Doppler half-widths of the absorber line and the emission line, respectively. The Doppler half-width is proportional to the square root of the Doppler temperature which leads to equation (4). The effective Doppler absorption cross-section, σ_e, is defined

$$\sigma_e = \sigma_0\{T_a/(T_a+T_e)\}^{0.5}. \tag{5}$$

Equation (1) can now be written as

$$S_o = \Sigma_i\langle E_i\rangle\{A\varepsilon T\eta\}\sigma_e L[O]. \tag{6}$$

Figure 1 is a schematic of the calibration system. It is a discharge bypass flow system of a nominal 15 cm i.d. aluminum tube which is large enough to wholly contain the instrument scattering volume. This tube is blackened with 3M black paint on the inside surface to reduce scattering. Ultra-high purity helium (99.9999%) is the main flow gas. The pressure at the midpoint of the tube length is measured with a thermocouple gauge. A mass flow transducer (Hastings) is used to find the flow velocity. The atom concentration is determined in two different ways in such a system.

The calibrations for the first flight reported here were done in the fast flow reactor at Harvard University where the quantities of ground state oxygen atoms were produced by the NO titration technique. Here known trace amounts of NO are added to a flow of N atoms, formed in a microwave discharge of N_2, giving ground state O atoms. The O atom concentration is proportional to the NO concentration when the reaction is driven to completion by excess quantities of N between the NO injection point and O atom detected point.

For the subsequent flights the University of Michigan flow system produced O atoms in a microwave discharge bypass of a trace amount of O_2 in a He carrier gas. The discharge is in an uncoated Pyrex tube which is also used as a movable atom injector into the center of the main He flow. The oxygen atom density is determined by an absorption experiment just upstream of the scattering volume using one of the lines from the 1304 Å multiplet produced in either a sealed lamp with two side arms, one containing $KMnO_4$ as an oxygen source and the other containing Ba as a getter, or a flowing lamp of He with a trace of O_2. Nominally the 1302 Å line is used. Opposite the lamp is a vacuum u.v. monochromater with a CsI cathode PMT detector. The field of view of the monochromater is reduced by the long evacuated tube to be an $f/35$ system.

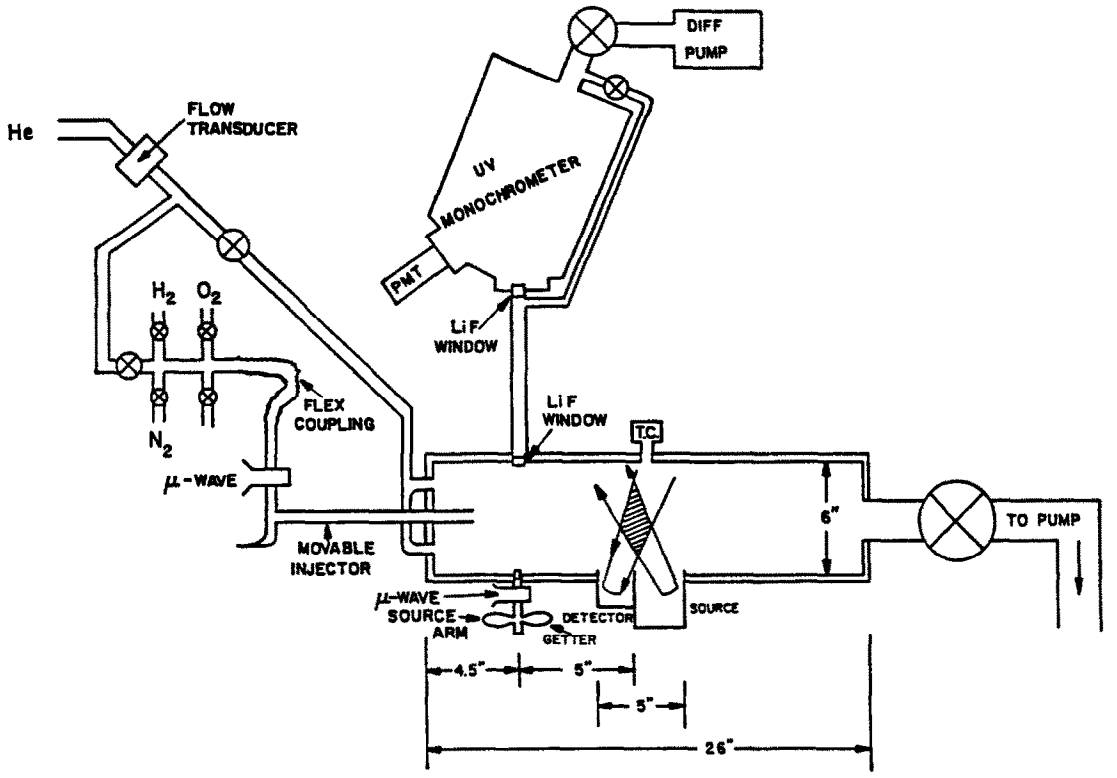

FIG. 1. THE CALIBRATION SYSTEM SHOWING THE GAS MANIFOLD, DISCHARGE BYPASS, MAIN FLOW CHAMBER WITH SENSOR SCATTERING VOLUME, AND ABSORPTION CELL WITH MONOCHROMATER.

Nominal flow conditions are a pressure of 1 torr and a flow velocity of 50 cm s^{-1}. When the injection point for the atoms is moved from near the sensor to the end wall, the observed sensor count rate decreases exponentially, indicating a wall removal rate (k_w) of 3.7 s^{-1}. This is consistent with a recombination efficiency of several times 10^{-4} for oxygen atoms on carbon-coated surfaces. The radial concentration gradients ($\Delta c/c$) are estimated from $\Delta c/c \sim r_0^2(k_v+3k_w)/8D$, where Δc is the concentration gradient between the center and wall of the tube, k_v and k_w are effective first order constants for volume and wall removal of atoms, r_0 the tube radius and D is the diffusion coefficient (Kaufman, 1961). For the case here $k_w \gg k_v$ and $D \sim 500$ cm^2 s^{-1} at 1 torr (Yolles and Wise, 1968) which gives $\Delta c/c \sim 0.16$. The atoms are considered to be nearly uniformly distributed across the diameter of the tube. However, this slight gradient will be considered in the error analysis.

The amount of absorption produced across the flow tube by various concentrations of O atoms (various optical depths) for optically-thin source lines was calculated using the equations developed by Mitchell and Zemansky (1934). However, Kaufman and Parkes (1970) have shown that the apparent optical depth is always less than the true optical depth when the absorption measurement is made using Doppler-shaped source lines having a finite optical thickness. Only in the limit of small optical depths in the absorber ($\tau < 1$) and the source ($\tau < 1$) does the apparent optical depth approach the true optical depth (correction less than 10%). Such an optical depth in the calibration source implies a partial pressure of oxygen of several millitorr. The departure of the three resonance line intensity ratios from their relative intensities at infinite temperature gives a measure of their optical depth. The observed ratios used in the absorption experiment were usually around 4.0:2.8:1 compared with the unreversed ratios of 5:3:1. The procedure outlined by Kaufman and Parkes (1970) is used to find the optical depth of the line being used in absorption and in all cases is found to be less than 0.1. The results of the absorption experiment were therefore not corrected for optical depth problems.

Oscillator strengths for the 1304 triplet have been

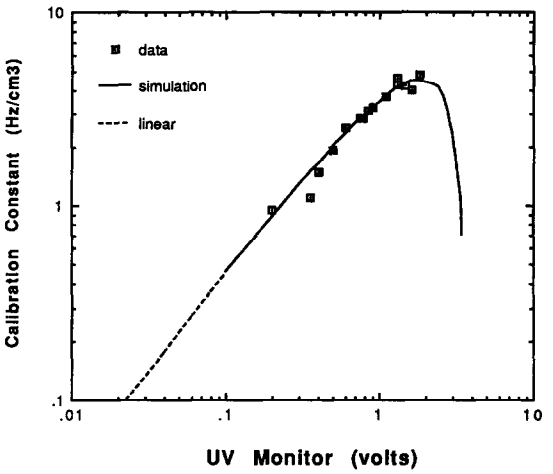

FIG. 2. THE CALIBRATION CONSTANT AS A FUNCTION OF FLUX FROM THE U.V. MONITOR.
The symbols are from the laboratory experiments. The continuous curve is from a theoretical simulation as discussed in the text.

measured a number of times. In particular, since 1968 the values have been between 0.045 and 0.053 (see Table 2 in Jenkins, 1985). A minimum variance was done on these 10 measurements and their errors. The result is an average $f = 0.047 \pm 0.001$. The oscillator strength was used to find the line center Doppler cross-section to be 1.6×10^{-13} cm^2. The effective absorption cross-section, equation (5), was calculated for T_e values of 300, 600, and 1000 K. The flow system was at room temperature and the absorption path was 17 cm. The absorption data and the effective cross-sections were used to find the [O] atom concentrations. Concentrations at the sensor of between 2 and 30×10^{10} cm^{-3} were used. An optical depth of one is produced in the flow by an atom concentration of 6×10^{11} cm^{-3}.

A concentration of O atoms was set to flow through the sensor scattering volume. The sensor source flux was increased by increasing the current to the source arm. Count rates of the detector were monitored as a function of the output voltage from the u.v. diode flux monitor. A background detector count rate could be determined by periodically turning off the O_2 admitted to the discharge bypass. The background count rate and u.v. diode flux monitor signal were found to be linearly proportional. The calibration factor was found to be nearly linearly proportional to the flux monitor voltage and increased as the flux was increased. A point was reached, however, where the calibration factor no longer increased for further increases in the source flux. Figure 2 illustrates a typical plot of calibration data. Here $C(E)$ is plotted as a function of increasing lamp flux and the region above 1 V on the u.v. monitor is the constant region. The continuous curve is a simulation of the scattering process for the instrument and will be discussed below.

The source flux was set for flight just below the point where the calibration factor no longer increased for increasing source flux (1 V in Fig. 2). The anticipated [O] in the mesosphere is of order 10^{11} cm^{-3}. The optical path to the scattering region and return from this region to the detector is 15 cm. Equation (5) is used to find the effective Doppler absorption cross-section using $T_a = 200$ K and $T_e = 2000$ K for the lamp beam (see below) and $T_e = 200$ K for the scattered beam. The optical depth can be calculated for the absorbed source lines to be less than 0.065 and for the absorbed resonantly scattered line to be about 0.2. Thus a single scattering experiment would result when the [O] was less than 2×10^{11} cm^{-3}. During the laboratory calibration, quantities of [O] in excess of 2×10^{11} were used to demonstrate that the fluorescence count rate vs oxygen atom density departed from linearity above 1.5×10^{11} cm^{-3}. Figure 3 illustrates this. These data show that for the densities of the oxygen peak region in the lower thermosphere the count rates will be lower than predicted on the basis of a linear relationship between count rate and density because of the increasing optical depth on the outward

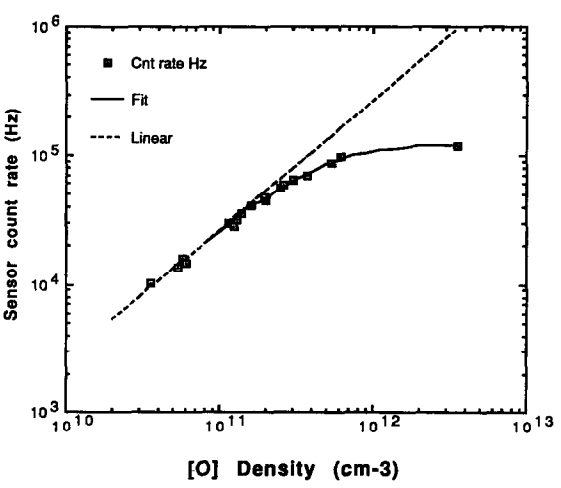

FIG. 3. THE DETECTOR COUNT RATE AS A FUNCTION OF ATOM DENSITY IN THE SCATTERING VOLUME.
The symbols are from the laboratory experiments. The line of constant slope (dashed) represents the optically thin scattering case. The solid line through the data is a guide to the eye and indicates the effects of increasing optical depth in the scattering volume.

bound lamp flux and the detector bound scattered flux. Thus the measurement could err on the side of too little [O], whereas it is unlikely that the [O] would be overestimated.

The emission temperature of the lamp is important for determining the effective absorption cross-section. A procedure for the determination of the emission temperature of a helium filled lamp has been outlined by Anderson *et al.* (1980). This involves setting a constant flow of [O] through the sensor scattering volume, heating the source arm such that the quantity of oxygen in the lamp is at a stable level, and then starting the discharge. From equation (6) it is obvious that the ratio of count rate to lamp flux at the initial turn-on to that obtained after the lamp is stabilized is given by

$$\frac{S_0/I_0}{S_t/I_t} = \frac{\sigma_{e0}}{\sigma_e} = \frac{\{T_{a0}/(T_{a0}+T_{e0})\}^{0.5}}{\{T_a/(T_a+T_e)\}^{0.5}}, \tag{7}$$

where $I = \Sigma_i \langle E_i \rangle$ and the "0" subscript is for $t = 0$. This procedure was done using helium and argon filled lamps. The assumption is made that at $t = 0$, $T_{a0} = T_{e0} = 300$ K and at $t = t$, $T_a = 300$ K. With this and the count rate flux ratios, T_e was determined to be about 2000 ± 1000 K for the helium lamp at 1 torr. The error is driven by the accuracy of the ratio at $t = 0$. Studies of lamps similar to this one by Rawlins and Kaufmann (1977) showed that for helium-filled lamps of 1 torr pressure operated at about 5 W r.f. power, the emission temperature was about 2000 K. The count rate flux ratio for an argon filled lamp gave Te about 8000 K. This is indicative that the discharge is probably created by energy transfer from Ar metastables which suggests a line that is not thermal (Kaufmann and Parkes, 1970).

SIMULATION

Having at hand the calibration of the lamp, it is instructive to compare it with a theoretical simulation of the lamp intensity and scattering process. The multiplet components are assumed to have an intensity of the form of a Type D lamp (Okabe, 1978):

$$E_i = E_{i0}\{1 - e^{-\tau_i}\} e^{-\tau_i'}, \tag{8}$$

where τ_i is the optical depth in the discharge region and τ_i' is the optical depth in an absorbing/non-emitting layer between the discharge and the lamp window through which the intensity emerges. It is this latter layer which can produce self reversal, a condition that has been shown to occur in the lamps when an intense output is desired (Dickinson *et al.*, 1980; Jenkins *et al.*, 1985). Equation (6) gives the relationship between the scattered intensity, S_0, and the optical depth in the scattering medium, $\sigma_e L$ [O], and the lamp intensity, $\Sigma\langle E \rangle$. Equation (6) was calculated using equation (8) as the intensity for each multiplet line. The temperature of the emitter line was 2000 K, the lamp absorber 350 K, and the scattering medium 300 K. The [O] was held fixed in the scattering medium at 10^{11} cm^{-3}. The results of the calculation are plotted as the solid line in Fig. 2. Since the calculation used an arbitrary excitation function, the results were normalized to the data between 0.4 and 1.0 V. The dashed line indicates the region where the source line is optically thin. The region of the solid line is where source self-absorption is increasing. That is why the slope of the curve decreases. The region of the maximum and rapid fall off is where the source is self-reversed.

The calibration factor also will allow an estimate of the lamp intensity I to be made for the experiment geometry. The flux reaching the scattering volume is related to the brightness of the source, B, by

$$E(\text{photons cm}^{-2}\,\text{s}^{-1}) = B\omega, \tag{9}$$

where ω is the solid angle subtended at the volume by the lamp discharge. For the optical design of the flight instrument, where the discharge is focused before the scattering volume,

$$\omega = A_s M^2/d^2, \tag{10}$$

where A_s is the area of the lamp aperture, M is the image magnification of the discharge, and d is the distance from the discharge image to the volume. Combining equations (2), (4), (5), (9), and (10), there results

$$C(E) = IM^2\sigma_e\varepsilon_D L/d^2, \tag{11}$$

where $\varepsilon_D = A\varepsilon T\eta$ is the detection efficiency and $I = BA_s$. Equation (11) can be written as

$$I(\text{photons s}^{-1}\,\text{sr}^{-1}) = C(E)\,d^2/\varepsilon_D\sigma_e L M^2. \tag{12}$$

The effective Doppler cross-section is calculated to be 5.8×10^{-14} cm^{-2} for the 1304 multiplet at an absorber temperature of 300 K and an emission temperature of 2000 K. The optical design gives a detection efficiency $\varepsilon_D = 3.7 \times 10^{-5}$, scattering length $L = 9.5$ cm, calibration constant $C = 4.4 \times 10^{-7}$ Hz cm^{-3}, source area $A = 0.48$ cm^2, magnification $M = 0.45$ and the distance from discharge image to scattering volume $d = 10$ cm. The result is $I = 1.1 \times 10^{13}$ photons s^{-1} sr^{-1}. This number is in good accord with other estimates from sealed sources (Okabe, 1964).

ERROR ANALYSIS

An estimate of the accuracy of the experiment involves error determination in the [O] concentration

at the sensor volume in the calibration system, the resulting count rate, the count rate during flight, and the source flux monitor. For a given [O], the calculated absorption produced across the flow tube has an accuracy of 5% based on the uncertainty in the effective Doppler temperature of the source line. There is also an estimated uncertainty of 10% in the absorption based on the degree of self-absorption in the source. The estimated accuracy in the measurement of the absorption is 7%. These result in an r.m.s. accuracy of 13% for the [O] determination at the absorption point. There is an additional uncertainty of 20% in the [O] at the flight instrument location because of uncertainty in the flow rates and system pressure. These give an estimate of an r.m.s. error of 24% for [O] at the flight sensor. The radial concentration gradient was shown to be 16% and the peculiar shape of the scattering volume (see Fig. 1) implies a non-uniform distribution of [O] atoms within it. The r.m.s. accuracy of the atom density within the scattering volume at the sensor is estimated to be 30%. The count rate produced by the [O] concentrations had an uncertainty of less than 3%. Consequently, the r.m.s. accuracy of the calibration of the sensor at room temperature is estimated to be 30%. The precision of the calibration before and after flight was 20%.

The calibration factor at an absorber temperature of 200 K, characteristic of the mesopause region, is 8% less then the factor measured at room temperature because of the temperature dependence of the effective cross-section. This is for a Doppler temperature of the emission line estimated to be 2000 K. An uncertainty in the mesopause temperature of 20 K results in a 5% uncertainty in calibration factor correction. The overall accuracy is thus 31%.

DATA

The oxygen resonance fluorescence module has been flown on the Michigan Airglow Payload 11 times during various geophysical conditions. During five of the flights the sensor failed to gather data because of data system or vehicle/mechanical failure. The successful data flights are listed in Table 1. On all of these experiments there were other sensors on board to gather data on the airglow emissions from the atmosphere that were produced by the odd oxygen recombination reactions (Siskind and Sharp, 1991; Sharp and Siskind, 1989) and by photon or electron impact on other constituents in the mesosphere/lower thermosphere.

To obtain the oxygen data the source lamp was switched on and off with a nominal period of 0.5 s. Within this period the on time was usually longer than the off time. In addition, for those flights when background was expected, the daytime and auroral flights, the detector viewed a thin, flat plate which was deployed. This was planned to reduce the background contribution but was not as successful as desired, for background signals still occurred.

Each payload was controlled by an attitude control system. The maneuvers of the payload were very similar from flight to flight. After the nose cone was deployed the control system pointed the payload axis tangent to the trajectory to within 4–6°. This orientation was held nominally until the payload was above 105 km when the payload axis would be pointed to the Earth's limb. The actual altitude at which this occurred varied from flight to flight. On payload descent through 105 km the payload axis was again tangential to the trajectory with the forward direction earthward. Again this point varied from flight to flight. The orientations tangential to the trajectory were done so that the angle of attack of the normal to the resonance fluorescence scattering plane was near 0°. Data are only considered for those cases where the angle of attack is within 10°. Usually across apogee data were obtained. Additionally, the sensor was always deployed on a boom to be greater than 60 cm from the payload.

The error bars which are placed on the figures of data discussed below are statistical. Below 100 km, generally, there is no background so the counts are from oxygen atoms and the error represents the counting statistics. When a background is present, the statistics of the data are determined from the difference of the counts when the lamp is on and when it is off. In the presence of the 1304 Å radiation in the dayglow and aurora, the scattered oxygen signal can be quite weak, so the statistical error becomes large.

13.135 *data*

The data published previously for this flight (Sharp, 1980) were incorrectly adjusted for temperature effects. Equation (5) for the effective cross-section had not been applied. In addition the count rate data near the peak concentration were not corrected for optical depth effects greater than 0.1. These corrections were made to the data and the corrected profile for the combination upleg and downleg data is shown in Fig. 4a. While the peak concentration remains at 94 km the concentration is now 1.9×10^{11} cm^{-3}. This is 1.7 times the previous value. The value of 1×10^{11} cm^{-3} is reached at 110 km. This new density will have an impact on the NO Delta band study of Rusch and Sharp (1981). The effect will be to reduce the atomic nitrogen density deduced by the corresponding amount. Also plotted in the figure is the MSIS oxygen

TABLE 1. INFORMATION ON EXPERIMENTS

Rocket No.	Date	Location*	SZA	$F_{10.7}$	A_p	[O] col. den.
13.135	2 Nov. 1978	WSMR	104°	152	10	350(15)†
4.339	8 Dec. 1981	WSMR	104°	287	15	347(15)
4.341	22 Sept. 1983	WSMR	52°	106	13	536(15)
33.056	17 Feb. 1987	WSMR	57°	68	9	400(15)
25.059	28 Mar. 1980	CRR	Aurora	203	7	240(15)
25.060	29 Nov. 1981	CRR	Aurora	204	15	240(15)

*WSMR: White Sands Missile Range (32.5°N, 106.5°W); CRR: Churchill Research Range (58.8°N, 94.3°W).

†Read 380(15) as 380×10^{15} cm^{-2}.

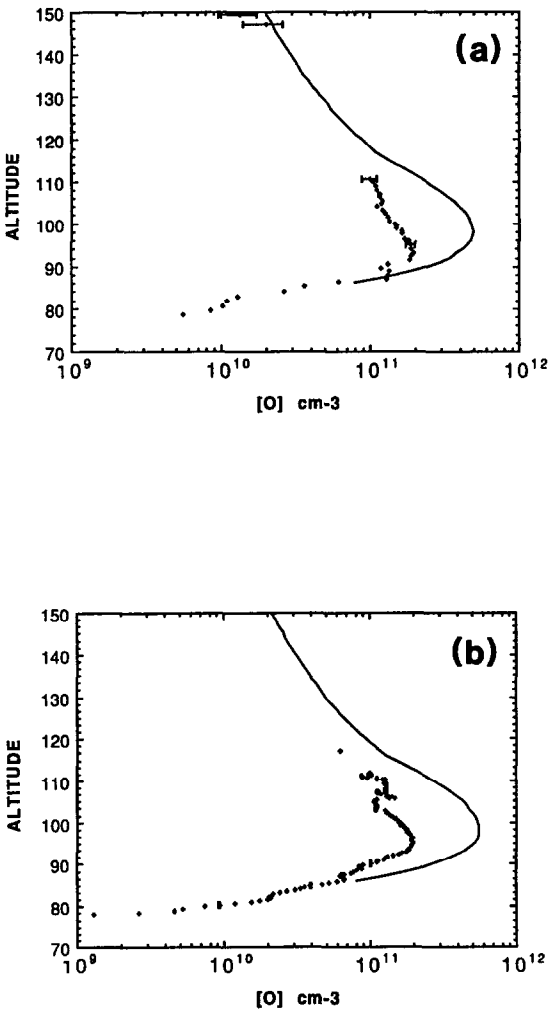

FIG. 4. THE ATOMIC OXYGEN MEASURED AT NIGHT. The symbols represent the data, the solid line the MSIS-86 model. The error bars are the 1 sigma counting statistics. (a) The data from 13.135. (b) The data from 4.339. The error is within the symbol because of the large counts (≈100,000 Hz).

calculated for the geographic and geophysical conditions. It is larger overall; however, it is within the measurement uncertainty at 148 km.

4.339 *data*

These data were obtained by an instrument module calibrated using the absorption technique. The upleg data are given in Fig. 4b. The downleg data were identical in concentration except that the structure was somewhat different. The peak density is 1.9×10^{11} cm^{-3} at 95 km. The density of 1×10^{11} cm^{-3} is reached by 110 km. The data stop at 117 km because this is the apogee of the payload. MSIS is plotted for the geophysical conditions on the launch day. The model clearly overestimates the density near the peak.

4.341 *data*

This is a daytime flight and the upleg data are given in Fig. 5a. There were no downleg data. The apogee for this flight was 125 km. The peak concentration is 3.2×10^{11} cm^{-3} at 100 km. The concentration of 1×10^{11} cm^{-3} is reached at 110 km. Notice that there is considerably more oxygen below 90 km, reaching a factor of 10 by 80 km, compared with the night-time data in Figs 4a and 4b. Again the MSIS overestimates the oxygen near the peak but is within the experimental error by 120 km.

33.056 *data*

The upleg data for this daytime flight are given in Fig. 5b where the peak density of 2.5×10^{11} cm^{-3} occurred at 99 km. There were no downleg data. The concentration of 1×10^{11} cm^{-3} is reached by the time the payload goes through 113 km. The data below 90 km are again enhanced relative to that from the night-time flights. The MSIS prediction for the time of the flight overestimates the peak density, but approaches the measurement by 115 km. The data stop at 125 km because the experiment was stopped to accommodate other instruments on the payload.

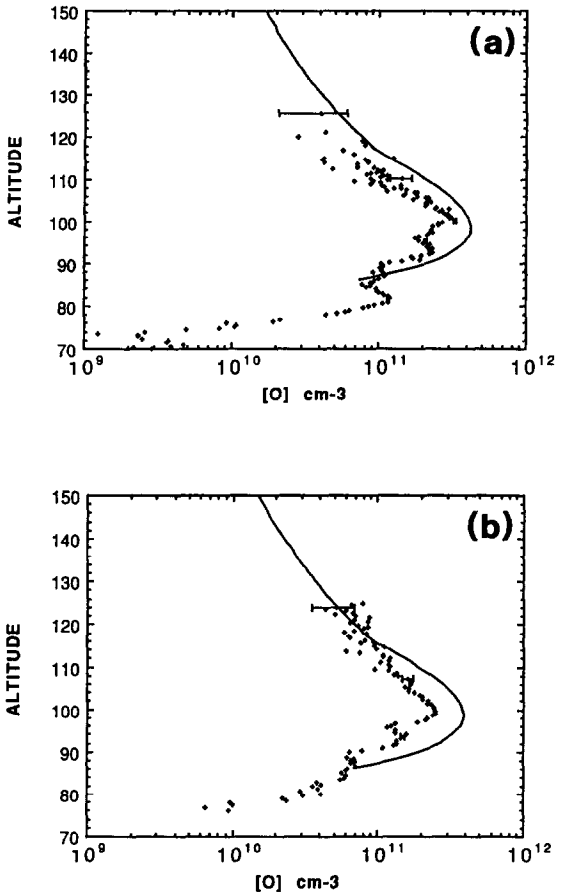

FIG. 5. THE ATOMIC OXYGEN MEASURED IN THE DAYTIME. The symbols represent the data, the solid line the MSIS-86 model. The error bars are the 1 sigma counting statistics. (a) The data from 4.341. (b) The data from 33.056.

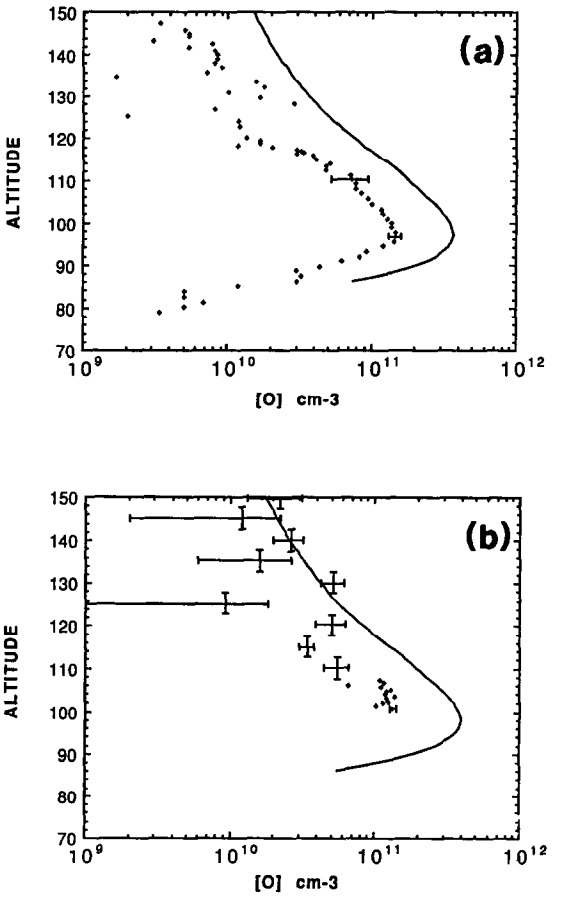

FIG. 6. THE ATOMIC OXYGEN MEASURED IN THE AURORA. The symbols represent the data, the solid line the MSIS-86 model. The horizontal error bars are the 1 sigma after subtraction of the background signal. The vertical bars are the bin sizes over which data were averaged. (a) The data of 25.059. (b) The data of 25.060.

25.059 *data*

These upleg data obtained in an aurora are given in Fig. 6a. The downleg data could not be calibrated because the intensity of the source started to increase at apogee beyond the calibration. The maximum concentration of 1.7×10^{11} cm^{-3} was reached at 97 km just prior to the boom being fully extended at 99 km. The density fell off quickly to 1×10^{11} cm^{-3} by 105 km. The large scatter in the data above 120 km is due to the accuracy of determining the scattered intensity in the presence of a large auroral 1304 Å multiplet signal. Note that the rapid decrease below the peak is similar to that for the midlatitude night-time data. The general nature of the altitude profile below the peak is that it is less than the midlatitude. The density above 130 km is considerably less than the data for 13.135 as well as the MSIS estimate. This is consistent with other studies which have inferred that the oxygen in aurora is less than models would predict in the thermosphere (Hecht *et al.*, 1989).

25.060 *data*

This additional set of auroral data is given in Fig. 6b. There were no downleg data. On this flight the absence of data below 100 km is due to the lamp being covered by a baffle prior to deployment. The data above 110 km had to be averaged because of the very intense auroral background which resulted in a signal-to-noise considerably less than unity. The vertical error bar indicates a 5 km binning for the average. The intent of the detector baffle was to reduce the background signal, but it was not as effective as

desired. The aurora was much brighter on this flight than for the 25.059 experiment. The density at 100 km is 1.4×10^{11} cm^{-3} decreasing to 1×10^{11} cm^{-3} at 105 km. Again the density is systematically lower than MSIS.

DISCUSSION

The overall shape of the profiles, while generally similar, is controlled by the local dynamics throughout and by photochemistry on the bottom side. While the peak density always occurs at some altitude, the dynamic control of the profile makes it difficult to assign a fixed altitude at which the peak always occur. Perhaps a more informative quantity would be the column content. This quantity was calculated for each flight. The column content below 110 km is listed in Table 1. For the 25.060 auroral experiment, the MSIS was adjusted to the data in order to obtain an extrapolation below 100 km. The four midlatitude profiles have an average column content of $4.1 \pm 0.4 \times 10^{17}$ cm^{-2}. This content is 40% larger than that which is deduced from the auroral data despite the fact that the maximum densities are similar. This suggests that the depletion of oxygen atoms extends throughout the lower thermosphere as well as the upper thermosphere when there is upwelling induced by particle and Joule heating.

The MSIS atomic oxygen is constructed in the lower thermosphere from the U.S. Standard Atmosphere 1976 oxygen profile. This profile is tied at 120 km to the MSIS estimate, so the absolute magnitude between 90 and 100 km is directly proportional to the magnitude at 120 km. The altitude of peak density would remain constant as well. The data reported here suggest that this may not be the true behavior, since for those profiles which approach the MSIS density above 120 km, there is still a considerable difference between the two in the region of the oxygen peak.

One-dimensional chemical/dynamic time-dependent models have reported estimates of the diurnal variation in minor constituents in the upper mesosphere (Allen *et al.*, 1984; Keneshea *et al.*, 1979). They predict day–night ratios of atomic oxygen at 80 km that are consistent with the measurements reported here; namely about a factor of 10.

All of the flights show wavelike structure on the profiles. Figure 7 is an enlargement of the low-altitude portion of the data from 4.339 and 4.341. The tick marks along the ordinate locate maxima in the shape of the profiles. Nominally the maxima separation is about 5 km. The altitude difference of about 5 km between the structures is consistent with those vertical lengths found by Kwon *et al.* (1987) in a study of sodium profiles measured by Lidar and which they attribute to the action of gravity waves.

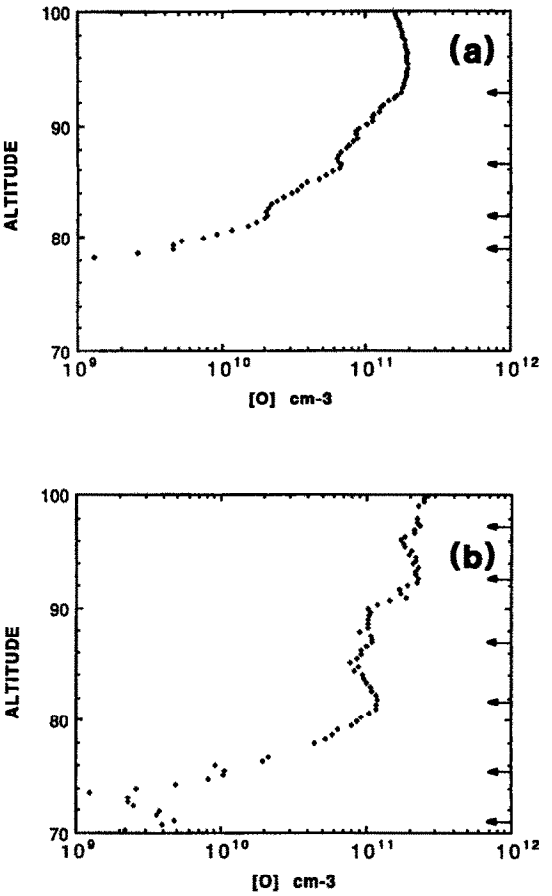

FIG. 7. THE BOTTOM SIDE OF THE DENSITY PROFILES FOR A NIGHT-TIME FLIGHT (4.339) AND A DAYTIME FLIGHT (4.341). The tick marks indicate where local maxima in the profiles occur. The gravity waves producing this structure have a nominal vertical wavelength of 5 km.

SUMMARY

A discussion of the laboratory calibration, calibration simulation, and accuracy of a resonance fluorescence module for measuring [O] atoms is given. This discussion demonstrates that a sensor can be calibrated with good accuracy to obtain *in situ* measurements of the [O] density in the mesosphere/lower thermosphere. [O] data have been obtained from six rocket flights. These data represent four midlatitude flights and two auroral flights. There are two night and two day profiles for the midlatitude experiments. The maximum densities found from this

set of data are between 1.5×10^{11} cm^{-3} and 3.5×10^{11} cm^{-3}. The data also show structure that is probably indicative of gravity wave effects of a nominal 5 km vertical wavelength.

Acknowledgement—Over the decade that the instrument has been developed and flown a number of people have made significant contributions. These are Prof. James Anderson and his group at Harvard University for help and advice in the calibration, and my engineers and students at the Space Physics Research Laboratory: Sepough Abedian, David Dettman, Walt Kargus, and Dieter Kita. The support for this research has been by NASA Grant NGR 23-005-360.

REFERENCES

Allen, M., Lunine, J. I. and Yung, Y. L. (1984) The vertical distribution of ozone in the mesosphere and lower thermosphere. *J. geophys. Res.* **89**, 4841.

Anderson, J. G., Grassl, H. J., Shetter, R. E. and Margitan, J. J. (1980) Stratospheric free chlorine measured by balloon-borne *in situ* resonance fluorescence. *J. geophys. Res.* **85**, 2869.

Bird, G. A. (1988) Aerodynamic effects on atmospheric composition measurements from rocket vehicles in the thermosphere. *Planet. Space Sci.* **36**, 921.

Dickinson, P. H. G., Bain, W. C., Thomas, L., Williams, E. R., Jenkins, D. B. and Twiddy, N. D. (1980) *Proc. R. Soc. Lond.* **A369**, 379.

Dickinson, P. H. G., Witt, G., Zuber, A., Murtagh, D., Grossmann, K. U., Bruckelmann, H. G., Schwabbauer, P., Baker, K. D., Ulwick, J. C. and Thomas, R. J. (1987) Measurements of odd oxygen in the polar region on 10 February 1984 during MAP/WINE. *J. atmos. terr. Phys.* **49**, 843.

Garcia, R. R. and Solomon, S. (1985) The effect of breaking gravity waves on the dynamics and chemical composition of the mesopause and lower thermosphere. *J. geophys. Res.* **90**, 3850.

Greer, R. G. H., Murtagh, D. P., McDade, I. C., Dickinson, P. G. H., Thomas, L., Jenkins, D. B., Stegman, J., Llewellyn, E. J., Witt, G., Mackinnon, D. J. and Williams, E. R. (1986) ETON 1: a data base pertinent to the study of energy transfer in the oxygen nightglow. *Planet. Space Sci.* **34**, 771.

Hecht, J. H., Christensen, A. B., Strickland, D. J. and Meier, R. R. (1989) Deducing composition and incident electron spectra from ground based auroral optical measurements: variation in oxygen density. *J. geophys. Res.* **94**, 13,553.

Hedin, A. E. (1987) MSIS-86 thermospheric model. *J. geophys. Res.* **92**, 4649.

Howlett, L. C., Baker, K. D., Megill, L. R., Shaw, A. W., Pendleton, W. R. and Ulwick, J. C. (1980) Measurement of a structured profile of atomic oxygen in the mesosphere and lower thermosphere. *J. geophys. Res.* **85**, 1291.

Jenkins, D. B. (1985) Oscillator strength of the 1304-nm OI triplet *J. quant. Spectrosc. radiat. Transfer* **34**, 55.

Jenkins, D. B., Watkins, G., Wareing, D. P., Freeman, G. H. C., Dickinson, P. G. H. and Mackinnon, D. J. (1985) Resolved line profiles of atomic oxygen resonance lamps used in the upper atmosphere. *J. quant. Spectrosc. radiat. Transfer* **34**, 123.

Kaufman, F. (1961) Reaction of oxygen atoms. *Prog. React. Kinet.* **1**, 1.

Kaufman, F. and Parkes, D. A. (1970) Sources of error in using resonance light absorption to measure atomic concentrations. *Trans. Faraday Soc.* **66**, 1579.

Keneshea, T. J., Zimmerman, S. P. and Philbrick, C. R. (1979) A dynamic model of the mesosphere and lower thermosphere. *Planet. Space Sci.* **27**, 385.

Kwon, K. H., Gardner, C. S., Senf, D. C., Roesler, F. L. and Harlander, J. (1987) Daytime lidar measurements of tidal winds in the mesospheric sodium layer at Urbana, Illinios. *J. geophys. Res.* **92**, 8781.

Llewellyn, E. J. (1988) The concentration of atomic oxygen in the mesosphere and the thermosphere. *Planet. Space Sci.* **36**, 892.

Llewellyn, E. J., McDade, I. C., Murtagh, D. P. and Witt, G. (1986) A comment on upper limits to [O] in the lower thermosphere. *Planet. Space Sci.* **34**, 393.

Mitchell, A. C. G. and Zemansky, M. W. (1934) *Resonance Radiation and Excited Atoms*, 92 pp. Cambridge University Press, New York.

Offerman, D., Friedrich. V., Ross, P. and Von Zahn, U. (1981) Neutral gas composition measurements between 80 and 120 km. *Planet. Space Sci.* **24**, 747.

Okabe, H. (1964) Intense resonance line sources for photochemical work in the vacuum ultraviolet region. *J. Opt. Soc. Am.* **54**, 47.

Okabe, H. (1978) *Photochemistry of Small Molecules*, p. 32. John Wiley, New York.

Rawlins, W. T. and Kaufman, F. (1977) Characteristics of O(I) and N(I) resonance line broadening in low pressure helium discharge lamps. *J. quant. Spectrosc. radiat. Transfer* **18**, 561.

Rusch, D. W. and Sharp, W. E. (1981) Nitric oxide delta band emission in the Earth's atmosphere: comparison of a measurement and a theory. *J. geophys. Res.* **86**, 10111.

Sharp, W. E. (1980) Absolute concentrations of O(^{3}P) in the lower thermosphere. *Geophys. Res. Lett.* **7**, 485.

Sharp, W. E. (1985) Upper limits to [O] in the lower thermosphere from airglow. *Planet. Space Sci.* **33**, 571.

Sharp, W. E. (1986) Reply to Llewellyn *et al. Planet. Space Sci.* **34**, 393.

Sharp, W. E. and Kita, D. (1987) *In situ* measurements of atomic hydrogen in the upper mesosphere. *J. geophys. Res.* **92**, 4319.

Sharp, W. E. and Siskind, D. E. (1989) Atomic emission in the ultraviolet nightglow. *Geophys. Res. Lett.* **16**, 1453.

Siskind, D. E. and Sharp, W. E. (1991) A comparison of measurements of the oxygen nightglow and atomic oxygen in the lower thermosphere. *Planet. Space Sci.* **39**, 627.

Thomas, R. J. and Young, R. A. (1981) Measurement of atomic oxygen and related airglows in the lower thermosphere. *J. geophys. Res.* **86**, 7381.

Yolles, R. S. and Wise, H. (1968) Diffusion and heterogeneous reaction, X. Diffusion coefficient measurements of atomic oxygen through various gases. *J. chem. Phys.* **48**, 5109.